J|A|C|S
ARTICLES
Published on Web 05/25/2007

Theory-Guided Design and Synthesis of Multichromophore Dendrimers: An Analysis of the Electro-optic Effect

Philip A. Sullivan,*,† Harrison Rommel,† Yi Liao,† Benjamin C. Olbricht,† Andrew J. P. Akelaitis,† Kimberly A. Firestone,† Jae-Wook Kang,‡ Jingdong Luo,‡ Joshua A. Davies,† Dong Hoon Choi,§ Bruce E. Eichinger,† Philip J. Reid,† Antao Chen,|| Alex K-Y. Jen,‡,† Bruce H. Robinson,*,† and Larry R. Dalton*,†

Contribution from the Department of Chemistry and Department of Materials Science and Engineering, University of Washington, Seattle, Washington 98105, Department of Chemistry, Korea University, Seoul, Korea, and Applied Physics Laboratory, University of Washington, Seattle, Washington 98105

Received November 20, 2006; E-mail: psull76@u.washington.edu; robinson@chem.washington.edu; dalton@chem.washington.edu

Abstract: Extensive experimental and theoretical study suggests that interchromophore electrostatic interactions are among the most severe impediments to the induction and stability of large electro-optic coefficients in electric-field-poled organic materials. In this report, multichromophore-containing dendritic materials have been investigated as a means to minimize unwanted attenuation of nonlinear optical (electro-optic) activity at high chromophore loading. The dendritic molecular architectures employed were designed to provide optimized molecular scaffolding for electric-field-induced molecular reorientation. Design parameters were based upon past experimental results in conjunction with statistical and quantum mechanical modeling. The electro-optic behavior of these materials was evaluated through experimental and theoretical analysis. Experimental data collected from the dendrimer structures depict a reasonably linear relationship between chromophore number density (N) and electro-optic activity (r_{33}) demonstrating a deviation from the dipolar frustration that typically limits r_{33} in conventional chromophore/polymer composite materials. The observed linear dependence holds at higher chromophore densities than those that have been found to be practical in systems of organic NLO chromophores dispersed in polymer hosts. Theoretical analysis of these results using Monte Carlo modeling reproduces the experimentally observed trends confirming linear dependence of electro-optic activity on N in the dendrimer materials. These results provide new insight into the ordering behavior of EO dendrimers and demonstrate that the frequently observed asymptotic dependence of electro-optic activity on chromophore number density may be overcome through rational design.

Introduction

Organic materials exhibiting large first nonlinear susceptibilities ($\chi^{(2)}$), and therefore, large electro-optic coefficients (r_{33}) have received considerable attention in recent years. Their development is motivated by the promise of performance and cost improvements related to telecommunications, computing, embedded network sensing, THz wave generation and detection, and many other applications.[1−4] High-speed electro-optical signal transduction (modulation) and routing (multiplexing) via the Pockels effect is attracting attention from computing and telecommunictions industries while terahertz wave technologies may find medical, analytical spectroscopy, and defense/homeland security applications. Organic second-order nonlinear optical, electro-optic (EO), materials have traditionally been prepared by incorporation of highly hyperpolarizable chromophores into a nonlinear optically inactive, polymeric host matrix.[5] The resulting chromophore/polymer composite materials are then heated near their glass transition temperatures under the application of an electric poling field to induce acentric ordering of the dipolar chromophores. Large EO coefficients (r_{33}) require a combination of high chromophore hyperpolarizability (β), chromophore number density per material unit volume (N), and efficient acentric molecular ordering. Extensive experimental and theoretical study has implicated interchromophore electrostatic (dipolar) interaction, guest−host incompatibility, and chromophore shape as major factors defining the electro-optic activity of electric field-poled organic materials.[6−8]

† Department of Chemistry, University of Washington.
‡ Department of Materials Science and Engineering, University of Washington.
§ Korea University.
|| Applied Physics Laboratory, University of Washington.

(1) Baehr-Jones, T.; Hochberg, M.; Wang, G.; Lawson, R.; Liao, Y.; Sullivan, P. A.; Dalton, L.; Jen, A. K. Y.; Scherer, A. *Opt. Express* **2005**, *13* (14), 5216−5226.
(2) Sinyukov, A. M.; Leahy, M. R.; Hayden, L. M.; Haller, M.; Luo, J.; Jen, A. K. Y.; Dalton, L. R. *Appl. Phys. Lett.* **2004**, *85* (24), 5827−5829.
(3) Schneider, A.; Gunter, P. *Ferroelectrics* **2005**, *318*, 83−88.
(4) Dalton, L. *Adv. Polym. Sci.* **2001**, *158*, 1−86.
(5) Prasad, P. N.; Williams, D. J. *Introduction to Nonlinear Optical Effects in Molecules and Polymers*; John Wiley and Sons: New York, 1991.
(6) Harper, A. W.; Sun, S.; Dalton, L. R.; Garner, S. M.; Chen, A.; Kalluri, S.; Steier, W. H.; Robinson, B. H. *J. Opt. Soc. Am. B* **1998**, *15* (1), 329−337.
(7) Dalton, L. R. *Pure Appl. Chem.* **2004**, *76* (7−8), 1421−1433.

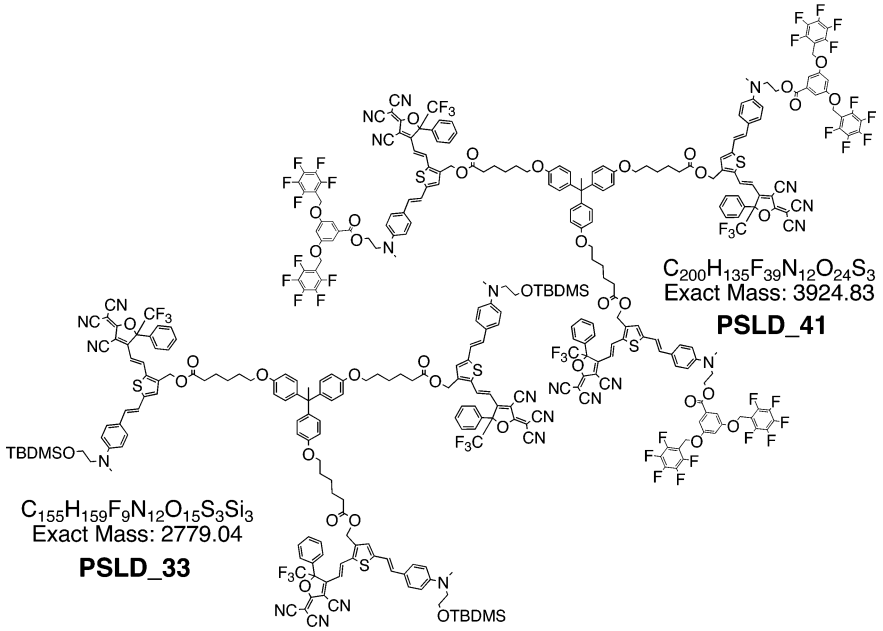

Figure 1. Three-arm EO dendrimers PSLD_33 and PSLD_41.

Because of magnified dipole−dipole electrostatic interaction, increased chromophore number density commonly impedes poling-induced molecular order, resulting in a maximum in the plot of electro-optic activity versus chromophore number density. Chromophore number densities greater than this optimum result in reduced poling-induced order, and thus lower r_{33}.[9]

To control the potentially detrimental effects of chromophore dipole−dipole interactions, material systems must be engineered at the molecular level employing first-principals theory-guided design. Molecular structure can be modulated through asymmetric organic synthesis, allowing control over electrostatic and other supramolecular interactions. Covalent modification may also be used to address compatibility problems through attachment of the chromophore to the host material or by creation of dendritic or hyperbranched molecular structures. Such well-designed molecular architectures have demonstrated significantly enhanced r_{33} as compared to analogous (e.g., containing the same fundamental π-electron core chromophore structure) guest−host blends.[10−13]

Multichromophore dendrimers are of particular interest because of the opportunities for molecular-scale architectural control. Alteration of chromophore and successive dendrimer generation binding geometry, attachment flexibility, and polarity can very effectively direct both intra- and intermolecular interactions.[14−18] Dendrimers display better overall mechanical stability and film-forming properties than small molecules, yet they retain many of the desirable characteristics inherent to small-molecule materials. Dendritic structures also offer unique characteristics such as globular shape, large internal free-volume, and an outer periphery capable of providing physical isolation of contents within. Theoretical analysis can be used as a guide in the bottom-up design of dendrimer materials which exploit these attributes to achieve greatly increased chromophore number density with no loss of poling-induced ordering efficiency.

The electro-optic properties of two multichromophore dendrimers were examined herein, and the effectiveness of theory-guided molecular engineering was examined. Multiple-chromophore-containing dendritic materials were used to fabricate stand-alone thin films with extremely high chromophore number density. These all-dendrimer films exhibit high poling efficiency, r_{33}/E_p. One of the most striking characteristics of the EO behavior displayed by the dendrimer materials is a linear dependence of r_{33} on N even when films were cast as pure dendrimer materials ($N = 6.45 \times 10^{20}$ chromophores/cc).

Synthetic Rationale

Previous work on mutlichromophore dendrimers focused on the optimization of intramolecular design parameters of three-arm dendritic chromophores.[19] In this report these previous findings have been employed to guide the design and synthesis of three-arm dendritic structures with extended outer peripheral functionality. These dendritic materials were designed for use in the fabrication of stand-alone amorphous thin films without the addition of an inert polymer host. Figure 1 illustrates the structures of the two three-arm dendrimers (PSLD_41 and PSLD_33), considered herein.

(8) Dalton, L. R.; Harper, A. W.; Robinson, B. H. *Proc. Natl. Acad. Sci. U.S.A.* **1997**, *94* (10), 4842−4847.
(9) Dalton, L. R.; Robinson, B. H. *J. Phys. Chem.* **2000**, *104*, 4785−4795.
(10) Briers, D.; Koeckelberghs, G.; Picard, I.; Verbiest, T.; Persoons, A.; Samyn, C. *Macromol. Rapid Commun.* **2003**, *24* (14), 841−846.
(11) Ma, H.; Liu, S.; Luo, J.; Suresh, S.; Liu, L.; Kang, S. H.; Haller, M.; Sassa, T.; Dalton, L. R.; Jen, A. K.-Y. *Adv. Funct. Mater.* **2002**, *12* (9), 565−574.
(12) Luo, J.; Haller, M.; Ma, H.; Liu, S.; Kim, T.-D.; Tian, Y.; Chen, B.; Jang, S.-H.; Dalton, L. R.; Jen, A. K.-Y. *J. Phys. Chem. B* **2004**, *108* (25), 8523−8530.
(13) Bai, Y.; Song, N.; Gao, J. P.; Sun, X.; Wang, X.; Yu, G.; Wang, Z. Y. *J. Am. Chem. Soc.* **2005**, *127* (7), 2060−2061.
(14) Ma, H.; Chen, B.; Sassa, T.; Dalton, L. R.; Jen, A. K.-Y. *J. Am. Chem. Soc.* **2001**, *123* (5), 986−987.
(15) Pereverzev, Y. V.; Prezhdo, O. V.; Dalton, L. R. *Chem. Phys. Lett.* **2003**, 373 (1,2), 207−212.
(16) Annoni, E.; Pizzotti, M.; Ugo, R.; Quici, S.; Morotti, T.; Bruschi, M.; Mussini, P. *Eur. J. Inorg. Chem.* **2005**, (19), 3857−3874.
(17) Yokoyama, S.; Nakahama, T.; Otomo, A.; Mashiko, S. *J. Am. Chem. Soc.* **2000**, *122*, 3174−3181.
(18) Gopalan, P.; Katz, H. E.; McGee, D. J.; Erben, C.; Zielinski, T.; Bousquet, D.; Muller, D.; Grazul, J.; Olsson, Y. *J. Am. Chem. Soc.* **2004**, *126* (6), 1741−1747.
(19) Sullivan, P. A.; Akelaitis, A. J. P.; McGrew, G.; Lee, S. K.; Choi, D. H.; Dalton, L. R. *Chem. Mater.* **2006**, *18*, 344−351.

Scheme 1. Synthesis Scheme for Three-Arm Dendrimers PSLD_33 and PSLD_41[a]

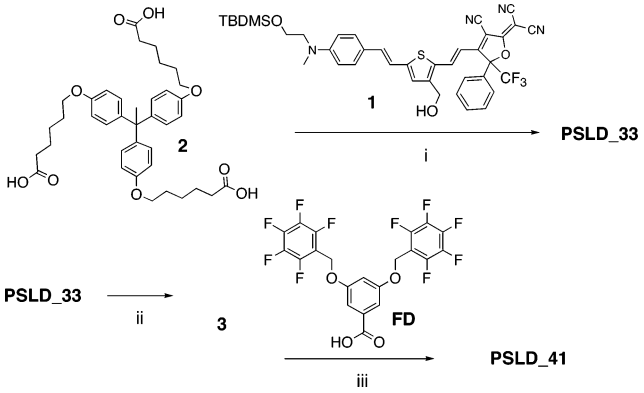

[a] Conditions: (i) DCC/DPTS, DCM/DMF, reflux 48 h, 50%; (ii) 1 N HCl (MeOH solution.), acetone, room temp, 2.5 h, quant.; (iii) DCC/DPTS, DCM/DMF, reflux 48 h, 62%.

Dendrimers PSLD_41 and PSLD_33 incorporate three chromophore units based on the CF_3-FTC design.[20−22] Synthetic details for the preparation of chromophore 1 can be found in Supporting Information. Both dendritic materials were synthesized following the outline in Scheme 1. Synthesis of the trihexanoic acid core has been reported previously.[19] Use of this core has been shown to lead to materials exhibiting excellent thermal and mechanical properties while allowing for efficient poling. Chromophore 1 (3 equiv) was introduced surrounding the core through esterification in the presence of DCC (*N*,*N*′-dicyclohexylcarbodiimide) and DPTS (4-(dimethylamino) pyridinium 4-tosylate) yielding tri-TBDMS (*t*butyl-dimethyl-silyl) functionalized three-arm dendrimer PSLD_33. The resulting material was then purified by silica gel column chromatography followed by reprecipitation from methanol. The TBDMS groups were then removed under mildly acidic conditions. The resulting trihydroxyl dendrimer was then functionalized with 3 equiv of the pentafluoro phenyl containing Frechet-type dendron (FD) to yield PSLD_41, which was again purified by similar means.[23] Synthetic material identity and purity was confirmed by ^{1}H NMR, MALDI-TOF mass spectrometry, and elemental analysis.

Theory

The order parameter $\langle \cos^n \theta \rangle$, for odd n, is a measure of dipolar order produced within the material matrix following the application of the poling field E_p. The order parameter depends on interchromophore electrostatic interactions, composite material component compatibility, covalent binding effects, molecular shape, and thermal randomization as well as other supramolecular interactions. At low density intermolecular electrostatic interactions are negligible compared to the dipole-field interaction and ordering is well-approximated by the Langevin functions:

$$\langle \cos^n \theta \rangle = \frac{f}{\sinh(f)} \frac{\partial^n}{\partial f^n} \left(\frac{\sinh(f)}{f} \right) \tag{1}$$

where the poling parameter is $f = \mu E_P / k_B T$. Inclusion of electrostatic interactions from neighboring chromophores attenuates the order parameters to values below that predicted by eq 1. The interaction with neighboring chromophores may be illustrated in terms of Piekara theory.[24,25] The poling parameter f is replaced by the interaction parameter z,

$$z^2 = f^2 + w^2 + 2fw \cos \Omega \tag{2}$$

where the dipole−dipole interaction parameter $w = (\mu^2/\bar{r}^3 k_B T)^2$ is related to the average nearest neighbor chromophore distance $\bar{r}$ and the angle Ω between the local dipolar field and the external poling field. Integration over Ω yields the expression for the order parameters:

$$\langle \cos^n \theta \rangle = \frac{1}{2} \int_\Omega \frac{z}{\sinh z} \frac{\partial \sinh z}{\partial z} \, d\Omega \tag{3}$$

At concentrations where dipole−dipole electrostatic interactions are dominant, the poling field may be treated as a perturbation in z; in this limit the order parameters $\langle \cos^n \theta \rangle$ exhibit a linear response to the strength of the poling field.

The material first nonlinear susceptibility, $\chi^{(2)}$ is directly proportional to electro-optic activity (r_{33}) expressed as

$$r_{33} = 2 \frac{N \beta_{zzz} F_L (3 - \lambda_{max}^2/\lambda^2)}{3\eta^4 (1 - \lambda_{max}^2/\lambda^2)} \langle \cos^3 \theta \rangle \tag{4}$$

where β_{zzz} is the first hyperpolarizability of individual chromophores,[5] N is the chromophore number density, η is the material index of refraction and the ratio $\lambda_{max}^2/\lambda^2$ refers to the wavelength at maximum absorbance to the wavelength of the incident light field. The local field correction $F_L = ((\eta_0^2(\eta_\omega^2 + 3))/(\eta_\omega^2 + 2\eta_0^2))(((\eta_\omega^2 + 2))/3)^2$ is the product of Lorentz and Onsager field factors for the static- and frequency-dependent refractive indices of the material.[5,26,27] The local field correction also modifies the effective poling field experienced by the chromophore,

$$E_p = \left(\frac{\eta_0^2 (\eta_\omega^2 + 3)}{\eta_\omega^2 + 2\eta_0^2} \right) E_0 \tag{5}$$

where E_0 is the magnitude of the applied (laboratory) poling field. The field correction factor could equally well be applied to the dipole moment, μ, in the μE_{pol} term. For the dendrimers considered in this study, where $\eta_0^2 \approx \eta_\omega^2 \approx 2.9$, the local poling field is approximately twice that of the applied field E_0.

Monte Carlo calculations are useful for predicting, in a semiquantitative fashion, the optimal order parameters for a given number density and poling field.[28] The molecular hyperpolarizability, β, may be estimated from quantum mechanical modeling and experimental measurement, yielding a quantitative prediction of r_{33} from first principles.[29,30] To model the bulk

(20) Liao, Y.; Anderson, C. A.; Sullivan, P. A.; Akelaitis, A. J. P.; Robinson, B. H.; Dalton, L. R. *Chem. Mater.* **2006**, *18* (4), 1062−1067.
(21) Xu, G.; Liu, Z.; Ma, J.; Liu, B.; Ho, S.-T.; Wang, L.; Zhu, P.; Marks, T. J.; Luo, J.; Jen, A. K.-Y. *Opt. Express* **2005**, *13* (19), 7380−7385.
(22) Paloczi, G. T.; Huang, Y.; Yariv, A.; Luo, J.; Jen, A. K.-Y. *Appl. Phys. Lett.* **2004**, *85* (10), 1662−1664.
(23) Luo, J.; Ma, H.; Haller, M.; Jen, A. K.-Y.; Barto, R. R. *Chem. Commun.* **2002**, (8), 888−889.
(24) Nielsen, R. D.; Rommel, H. L.; Robinson, B. H. *J. Phys. Chem. B* **2004**, *108* (25), 8659−8667.
(25) Piekara, A. *Proc. R. Soc. London, Ser. A.* **1939**, *172*, 360.
(26) Zyss, J.; Chemla, D. S., *Nonlinear Optical Properties of Organic Molecules and Crystals*; Academic Press: New York, 1987; Vol. 1, p 97−99.
(27) Onsager, L. *J. Am. Chem. Soc.* **1936**, *58* (8), 1486−1493.
(28) Robinson, B. H.; Dalton, L. R. *J. Phys. Chem. A* **2000**, *104* (20), 4785−4795.
(29) Firestone, K. A.; Reid, P.; Lawson, R.; Jang, S.-H.; Dalton, L. R. *Inorg. Chim. Acta* **2004**, (357), 3957−3966.

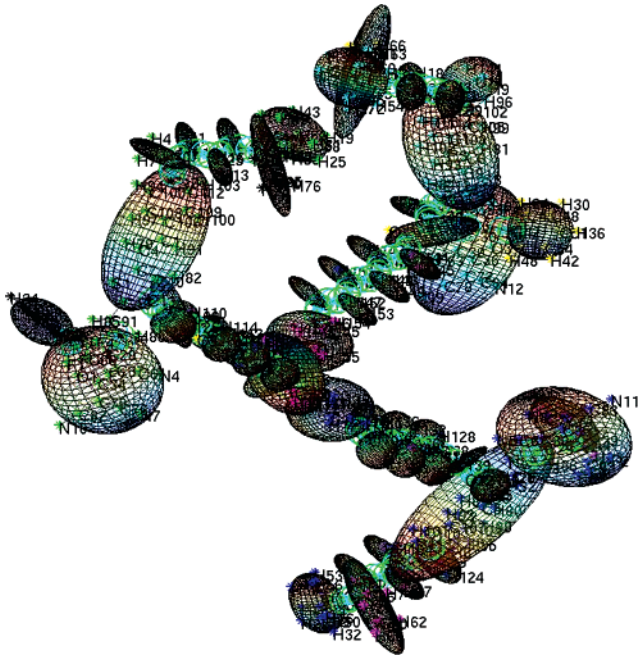

Figure 2. The three-arm dendrimer PSLD_33 represented as a system of ellipsoids. Green circles show where the rotations between ellipsoids may occur.

ordering in complicated dendrimeric systems, we have constructed a coarse-grained, united atom model based on the PSLD_33 dendrimer/chromophore system (Figure 2). A fully atomistic statistical calculation is computationally intractable; hence, we have partitioned the dendrimer into ellipsoidal subdomains. Ellipsoids are traced about the atom positions, which are optimized structures generated by density functional theory (DFT). The ellipsoids are allowed complete rotational freedom, except for the three that together comprise the active chromophore, about the bonds within the molecule. Each ellipsoid is assigned a Lennard-Jones type potential and dipole moments are placed within the ellipsoids corresponding to the principal chromophore axes. We use the contact function of Perram and Wertheim[31] to calculate ellipsoidal overlap. The contact function allows a precise knowledge of the minimum surface to surface distance between ellipsoids which is then mapped onto a modified Lennard-Jones potential,

$$U_{\mathrm{LJ}} = \frac{4}{k_{\mathrm{B}}T}\sum_{i<j}\sigma_{ij}\left[\left(\frac{R_{ij}^{o}}{R_{ij}}\right)^{12} - \left(\frac{R_{ij}^{o}}{R_{ij}}\right)^{6} + \frac{A_{\mathrm{sol}}}{2}\left[1 - \tanh\left(\frac{R_{ij} - 2^{1/6}R_0 - d}{d}\right)\right]\right] \quad (6)$$

The sum is over all neighboring ellipsoids where contact and overlap are possible. R_{ij} is the center-to-center distance between ellipsoids i and j. R_{ij}^{o} is the center-to-center distance between ellipsoids i and j when the two ellipsoids are just touching and σ_{ij} is the energy minimum. In the calculations the empirical parameters $A_{\mathrm{sol}} = 1$ and $d = 2$ Å serve to attenuate the Lennard-Jones energy minimum to produce a smoothly repulsive potential without the discontinuity associated with a hard-core/step function approach.

The total thermal energy of the system is given by the sum of Lennard-Jones, dipole-field and dipole−dipole interactions,

$$U_{\mathrm{T}} = U_{\mathrm{LJ}} + \frac{1}{k_{\mathrm{B}}T}\left[\sum_{j} - \mu E_{\mathrm{P}}\cos\theta_j + \sum_{i<j}\frac{\vec{\mu}_i\cdot\vec{\mu}_j}{r_{ij}^{3}} - 3\frac{(\vec{\mu}_i\cdot\vec{r}_{ij})(\vec{\mu}_j\cdot\vec{r}_{ij})}{r_{ij}^{5}}\right] \quad (7)$$

where θ_j is the angle of the jth chromophore with respect to the poling field director. Characters with an arrow denote vector quantities. In the course of a Monte Carlo calculation the summation is over all effective neighbors using the minimum image convention with respect to the simulation cell and the traditional Metropolis algorithm for configuration acceptance.[32]

When studying the effects of molecular shape on electric field-induced dipolar order, models of spherical point dipoles serve as an ideal benchmark against which to compare more complicated systems, such as dendrimeric chromophores. Two theoretical models, on-lattice and off-lattice, were explored to examine the poling-induced ordering behavior of the spheres. In the on-lattice model, spheres are only allowed to rotate, holding their translational positions fixed. The off-lattice model allows for both translational and rotational molecular motion while the system approaches a minimum energy state. The dipole moment for the chromophores is set to 12 Debye, and the poling temperature is 350 K. The local poling field is set to 300 V/μm. For the off-lattice calculations, each sphere is assigned a modified Lennard Jones energy of $\sigma_{ij}/k_{\mathrm{B}}T = 0.2$.

Figure 3 shows the calculated order parameters for on-lattice and off-lattice models as a function of density for spheres, each containing a single dipole at the center. Ordering is greater in the off-lattice case (black) than for the simple cubic lattice (blue). FCC (red) and BCC (green) lattice geometries show intermediate ordering. Both $\langle\cos\theta\rangle$ and $\langle\cos^3\theta\rangle$ are shown. It is apparent from the figure that $\langle\cos^3\theta\rangle \approx 0.6\langle\cos\theta\rangle$ irrespective of N. This observation suggests that the assumption that $r_{33} = 3r_{13}$, commonly used in ellipsometric r_{33} measurements, is valid for practical poling voltages and realistic N values.

Results and Discussion

UV−visible absorption spectroscopy performed on the two dendrimers PSLD_33 and PSLD_41 yielded the physical parameters listed in Table 1. Also shown are thermal data obtained using differential scanning calorimetry (DSC). Dendrimers PSLD_33 and PSLD_41 displayed distinct glass-transition temperatures of 85 and 103 °C, respectively. The absorption maxima corresponding to each compound, both from a solution in chloroform and from a thin solid film were evaluated and tabulated. Both PSLD_33 and PSLD_41 were spin cast on glass slides as solutions of pure compounds. Decreased solvatochromic dependence is apparent for PSLD_41 in going from solution to film. Attenuated solvatochromic shift implies that the chromophore units comprising PSLD_41 are

(30) Kinnibrugh, T.; Bhattacharjee, S.; Sullivan, P.; Isborn, C.; Robinson, B. H.; Eichinger, B. E. *J. Phys. Chem. B* **2006**, *110*, 13512−13522.
(31) Perram, J. W.; Wertheim, M. S. *J. Comp. Phys.* **1985**, *58*, 409.
(32) Allen, M. P.; Tildesley, D. J. *Computer Simulation of Liquids*; Oxford University Press: New York, 1987.

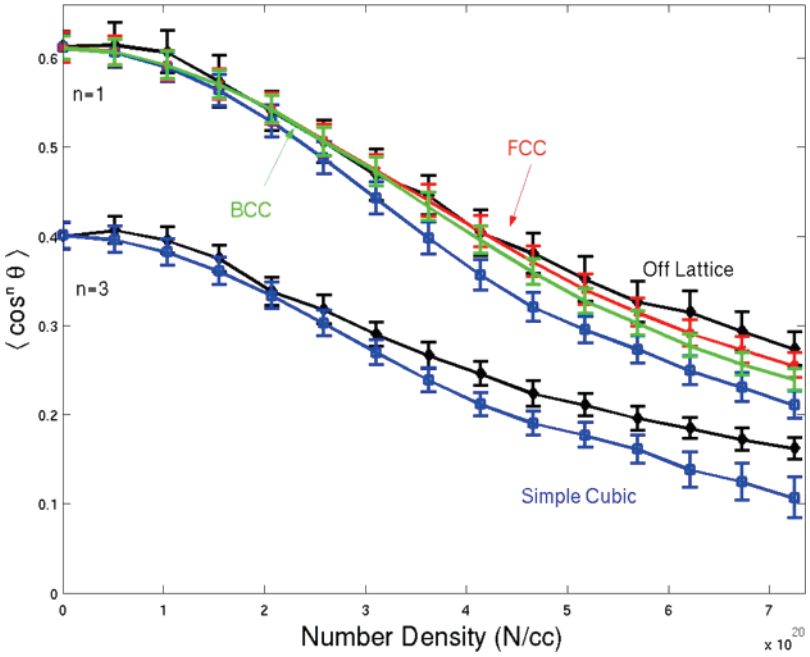

Figure 3. Monte Carlo predicted behavior of order parameter as a function of number density as calculated for dipoles contained in a spherical shell. Results are shown for both on-lattice and off-lattice models (black lines).

Table 1. Thermal and UV−Visible Absorption Data for EO Dendrimers

compound	T_g (°C)	λ_{max} ($CHCl_3$) nm	λ_{max} (film)[a] nm
PSLD_41	103	724	720
PSLD_33	96	759	734

[a] Absorption maximum of a neat dendrimer thin-film cast on glass

effectively shielded from the surrounding environment by the extended peripheral structure.[33]

Evaluation of the electro-optic properties of pure films of PSLD_33 and PSLD_41 was performed using a modification of the widely utilized single-beam reflection ellipsometry apparatus. The instrument was modified to simultaneously monitor the EO-modulated signal intensity (I_m) and unmodulated probe intensity (I_c) in real-time during poling.[19,34,35] Such modification allowed in-situ optimization of processing conditions. Samples of each material were prepared by solution spin-casting onto ITO (indium tin oxide transparent electrode) coated glass slides. Gold electrodes ($d \approx 200$ nm) were then deposited atop the films. EO measurements were performed at a probe wavelength of $\lambda = 1310$ nm. After cooling and removal of the poling field, r_{33} values were calculated by sine wave fitting of lock-in-amplifier and direct detector response curves as a function of the relative phase angle (Ψ_{sp}) between T_E and T_M modes of the exciting light field.

The experimental r_{33} measurement results corresponding to PSLD_33 and PSLD_41 are depicted in Figure 4. The slope of a linear plot of r_{33} with respect to electric field, E_p (V/μm), (applied at optimum poling temperature) defines the poling efficiency, r_{33}/E_p, of a given material. Experimental error can be approximated as 15−20% owing to the combination of film

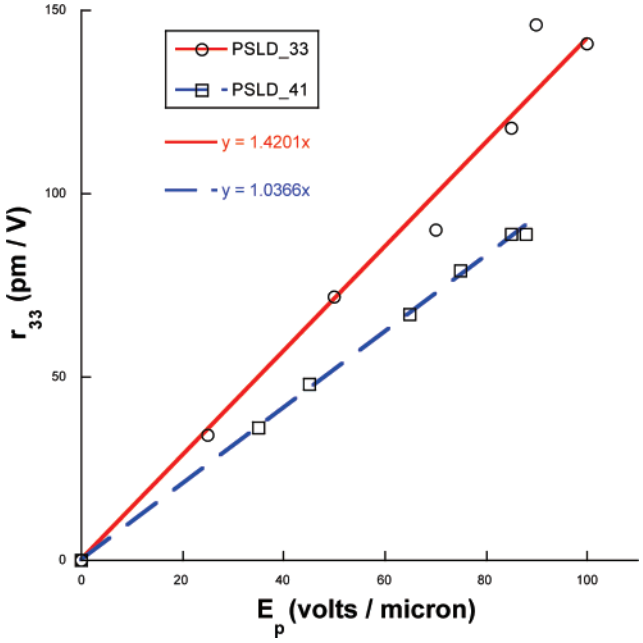

Figure 4. Experimental r_{33} data for PSLD_33 and PSLD_41 pure films as a function of applied poling voltage. Poling efficiency is determined as the slope; $r_{33}/E_p = 1.42$ and 1.04 $(nm/V)^2$ for PSLD_33 and PSLD_41, respectively.

thickness, E_p, and r_{33} measurements. Poling efficiency determines the r_{33} obtained through application of a known poling voltage. However, maximum r_{33}/E_p ratio does not necessarily guarantee maximum EO activity. Secondary material properties such as decreased resistivity often also depend on N and can limit the maximum E_p that can be applied before dielectric breakdown occurs.

The r_{33}/E_p ratios measured for films of PSLD_33 and PSLD_41 were determined as 1.42 and 1.04 $(nm/V)^2$, respectively (Figure 3). Our previously reported EO value for the parent chromophore, CF_3−FTC in APC (poly[bisphenol A

(33) Frechet, J. M. J.; Hawker, C. J.; Gitsov, I.; Leon, J. W. *J. Macromol. Sci., Pure Appl. Chem.* **1996**, *A33* (10), 1399−1425.
(34) Michelotti, F.; Toussaere, E.; Levenson, R.; Liang, J.; Zyss, J. *Appl. Phys. Lett.* **1995**, *67* (19), 2765−2767.
(35) Michelotti, F.; Toussaere, E.; Levenson, R.; Liang, J.; Zyss, J. *J. Appl. Phys.* **1996**, *80* (3), 1773−1778.

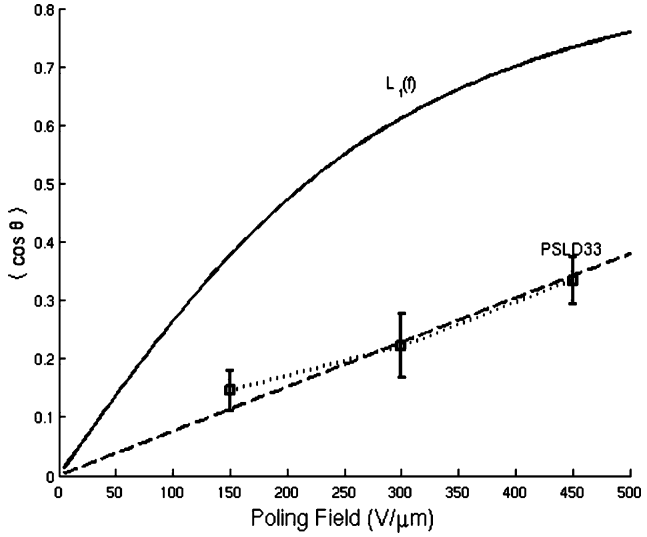

Figure 5. Order parameter $\langle\cos\theta\rangle$ of PSLD_33 as a function of field strength (squares), Langevin limit (solid line) where $\langle\cos^3\theta\rangle \approx 0.6\langle\cos\theta\rangle$

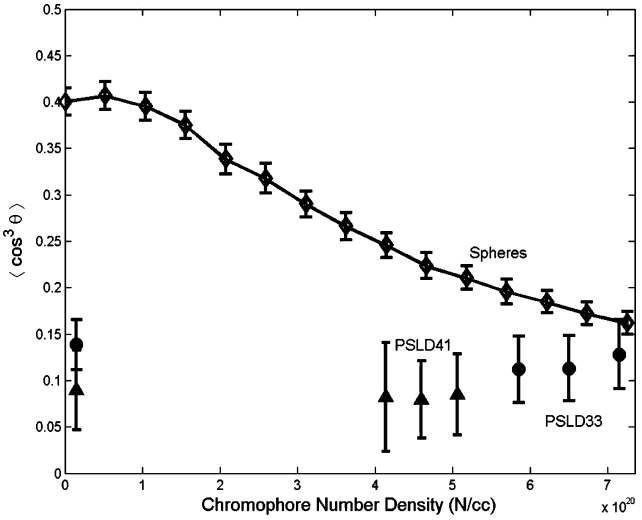

Figure 6. MC predicted behavior of $\langle\cos^3\theta\rangle$ as a function of N for dipolar spheres (diamonds), PSLD_33 (circles), and PSLD_41 (triangles) dendrimers. The error bars represent the standard error of the $\langle\cos^3\theta\rangle$ averaged over the set of trajectories.

carbonate-co-4,4′-(3,3,5-trimethylcyclohexyl-idene)diphenol carbonate]) host polymer, at optimum loading of $N = 1.78 \times 10^{20}$ chromophores/cc, was $r_{33}/E_p = 0.45$ (nm/V).[220] Compared to this optimized value for the same fundamental π-electron core chromophore structure in a polymer host, PSLD_33 exhibits an r_{33}/E_p ratio that is enhanced by a factor of 3. The increase in poling efficiency displayed by the PSLD_41 ($N = 4.6 \times 10^{20}$ chromophores/cc) and PSLD_33 ($N = 6.45 \times 10^{20}$ chromophores/cc) samples was found to be approximately proportional to increased chromophore number density. Optimized r_{33} values for PSLD_33 and PSLD_41 were found to be 140 and 90 pm/V, while the value for CF_3-FTC in APC was previously reported as 52 pm/V.[20]

Simulations were carried out (in parallel with experiments) to determine the origins of the more than 3-fold enhancement in r_{33}/E_p observed for dendrimer films relative to the analogous chromophore as an APC composite. For the simulation, *NVT* Monte Carlo calculations were performed on multiellipsoidal structures generated from the dendrimers PSLD_33 and PSLD_41. The results were referenced against those predicted for dipolar spheres. Systems were constructed using $N = 64$ molecules with periodic boundary conditions. This corresponds to systems of 3520 and 4864 ellipsoids in the simulation cell for the PSLD_33 and PSLD_41 systems, respectively. For all the following dendrimer calculations, order parameters were computed by assembling the final 5000 equilibrated NVT MC trajectories from 25 runs. Average values and standard deviations were then calculated from the resulting assembled trajectories. The dipole moment for the chromophores was set to 12 Debye, and the poling temperature was 350 K. Unless otherwise noted, the local field was set to 300 V/micron corresponding to a laboratory poling field of 150 V/micron. For MC simulations of both PSLD_41 and PSLD_33 the parameters $\eta^2 = 2.9$, $\lambda_{max} = 700$ nm, $\lambda = 1300$ nm, and $\beta_{zzz} = 3200 \times 10^{-30}$ esu, were used in conjunction with eq 4 to yield an estimate of r_{33}. While the experimentally determined values for PSLD_33 and PSLD_41 differ slightly from the parameters chosen, these values in addition to the local field E_p were set as identical in the simulations to isolate the effects of ordering due to the differences in the local steric environment.

MC calculations were carried out to determine the effect of the poling field strength on the linear order parameter of the three-arm dendrimer PSLD_33. Langevin theory predicts a nonlinear response in the field for typical values of the poling parameter. However the MC results show that the order parameter does follow linearly with poling field strength (Figure 5) consistent with the expected order from Piekara theory when dipole−dipole interactions are dominant. Figure 5 plots the order parameter $\langle\cos\theta\rangle$ as a function of poling field strength for the PSLD_33 dendrimer ($\langle\cos^3\theta\rangle \approx 0.6\langle\cos\theta\rangle$). The solid line represents the order predicted by dilute (Langevin) theory for dipolar spheres. The dashed line represents a least-squares best fit through the calculated values for PSLD_33 and the origin. For all calculations the density is set to 0.9 g/cm^3 ($N = 5.9 \times 10^{20}$ chromophores/cc). At this density the possibility exists for contribution of both intra- and intermolecular electrostatic interactions to the attenuation of the order parameter. The linear response to the poling field predicted by simulation reproduces the general behavior of r_{33} with respect to E_p presented above.

Figure 6 shows the order parameter, $\langle\cos^3\theta\rangle$, as a function of number density for the three-arm dendrimers PSLD_33, and PSLD_41. The order parameter of the dipolar spheres was also computed for comparison. The triad of results for each of the dendrimers, shown for the higher density measurements, $4 \times 10^{20} \le N \le 8 \times 10^{20}$ cc^{-1}, represent material densities of 0.9, 1.0, and 1.1 g/cm^3. This density range was investigated to explore potentially different dendrimer densities. Unlike the dipolar spheres, no tendency is predicted for the dendrimers to approach the Langevin-like order parameter at low N. Order parameters predicted for the two dendrimers remain virtually constant over the relevant range of N. This suggests that intramolecular interactions within single dendrimer molecules play a major role in determining the net dipolar order. Such behavior implies that at low dendrimer concentration, although overall chromophore N may be diluted by dispersion of the dendrimer into an inert host, high local chromophore N is maintained due to the covalent attachment of three chromophore units, limiting maximum interchromophore separation. At high dendrimer concentration, as is the case for pure dendrimer films,

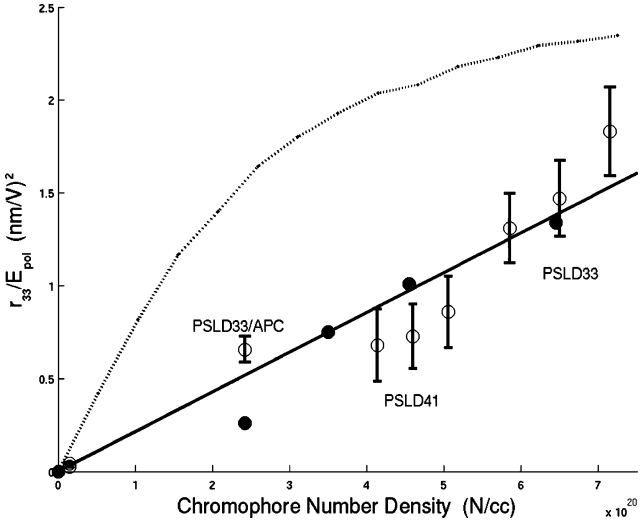

Figure 7. Monte Carlo simulations of r_{33}/E_p, assuming $\mu = 12$ Debye, $E_p = 150$ V/μ and $\beta_{zzz} = 3200 \times 10^{-30}$ esu for the two different dendrimers at different number density (open circles). Dipolar spheres are shown for reference (dotted line). The error bars are the standard error of the MC simulations. Experimental measurements for dendrimer samples are the solid circles, and the straight line is the best proportional fit, only to aid the eye.

the opposite scenario can be envisioned. High N MC results for the dendrimers suggest that minimum interchromophore distance is also limited, so that increased densities have little effect on intermolecular interactions reflecting little dependence of $\langle\cos^3\theta\rangle$ on N. Such limitations are not apparent for independent dipolar spheres in which the average interdipole distance may be widely varied leading to a pronounced $\langle\cos^3\theta\rangle$ dependence on N. The calculation of the order parameter shows that it is nearly independent of N. It follows from eq 4 then that r_{33} will be proportional to N if the other parameters, such as the molecular hyperpolarizability, remain constant.

Figure 7 shows the experimental data points for two pure dendrimer films (assuming a density of 1 gram/cc). Additionally, shown in Figure 7, are two lower N dendrimer compositions prepared by dispersing PSLD_33 into an APC polymer host at 2.4×10^{20} and 3.5×10^{20} active chromophore molecules (three for each dendrimer) per cubic centimeter of material. The plot of r_{33}/E_p is approximately proportional to N, with some data scatter. Such behavior is consistent with the trend expected from MC simulations. The experimental poling efficiency ratio of PSLD_33 to PSLD_41 dendrimers was found to be approximately 1.4, matching well the ratio of 2 found by MC calculations. Figure 7 shows the dependence of r_{33}/E_p for the simulation of simple dipolar spheres, using the same parameters. The nonlinear nature of the dependence on N for the dipolar spheres illustrates the qualitative difference of this model and the fact that dipolar spheres cannot adequately model the experimental data.

Theoretical simulation of r_{33}/E_p requires an estimate of both the order parameter and the molecular hyperpolarizability, β_{zzz}. The best overall single value used to compare with the experimental data is $\beta_{zzz} = 3200 \times 10^{-30}$ esu. This value is larger than that calculated from DFT theory in vacuo but compares favorably with the experimentally determined β_{zzz} measured in chloroform solution. Hyperpolarizability may be determined from the experimentally measured $\beta_{HRS} = (1183 \pm 130) \times 10^{-30}$ esu for CF_3−FTC, as evaluated in-house by hyper-Raleigh-scattering at an excitation wavelength of $\lambda = 1.0$ μm.[29,36] The relative HRS intensity was converted to absolute units via internal reference to chloroform, using the literature value of $\beta_{CHCl_3} = (0.16 \pm 0.008) \times 10^{-30}$ esu.[37] To estimate β_{zzz} from β_{HRS} for a dipolar chromophore where β_{zzz} is much greater than all other components of the hyperpolarizability tensor, the Cyvin−Rauch−Decius treatment yields the conversion: $\beta_{HRS} \approx 0.414\beta_{zzz}$.[38] This relation gives an experimentally based estimate of $\beta_{zzz} = 2857 \times 10^{-30}$ esu that compares very favorably with the best-fit value determined above.[30] As one can see, this value spans the data range reasonably well, being too large for the PSLD_33 and too small for the PSLD_41, and also too large for the PSLD_33/APC.

Conclusions

We have shown that theory-guided modification of EO chromophores from that of the traditional prolate ellipsoidal geometry can yield robust r_{33} coefficients owing to the enhancement of chromophore density beyond that obtainable by unmodified chromophores in a polymer matrix. A simple model of dipole−dipole, dipole-field, and steric interactions presents a semiquantitative description of the behavior of these novel molecules. While there is a need for further refinement of the coarse grained MC calculations, we have captured the essential elements of the physics behind the behavior and ordering of sterically modified (dendritic) chromophores. Theory has shown that the order parameter for the dendrimer systems is nearly constant with number density and that the PSLD_33 consistently has a modestly higher EO response (around 50% higher) than PSLD_41. These results are consistent with the experimental finding. While the value of the hyperpolarizability is somewhat unknown, it is encouraging that a best-fit value is nearly the same as that estimated from the HRS experiments. The assumption that a single hyperpolarizability is valid for all experimental conditions may prove to be too approximate.

The MC simulations, as reported, do not consider the dielectric properties of the bulk material (pure dendrimer), which implies that the dielectric constant carries a value of unity. Currently, we believe that the correct, unmodified, gas-phase dipole moment is actually 24 D (consistent with QM calculations performed using four different methods).[39] The work presented uses an effective dipole moment of 12 D. Our calculations of order yield identical order parameters when the dipole moment is doubled (24 Debye) and the poling field is halved (150 V/micron, the experimental value) and when a dielectric constant of 4 is used in the calculations when considering interchromophore, dipole−dipole, electrostatic interactions. This point, which is beyond the scope of the current discussion, also has implications for the quantum mechanical prediction of hyperpolarizability and will be addressed in detail elsewhere. Experiments are currently underway to explore the possibility that the intrinsic hyperpolarizability, in addition to dipole moment, exhibits a dependence on the nature of the molecular environment.

(36) Liao, Y.; Eichinger, B. E.; Firestone, K. A.; Haller, M.; Luo, J.; Kaminsky, W.; Benedict, J. B.; Reid, P. J.; Jen, A. K. Y.; Dalton, L. R.; Robinson, B. H. *J. Am. Chem. Soc.* **2005**, *127* (8), 2758−2766.
(37) Kaatz, P.; Shelton, D. P. *Opt. Commun.* **1998**, (157), 177−198.
(38) Cyvin, S. J.; Rauch, J. E.; Decius, J. C. *J. Chem. Phys.* **1965**, *43* (11), 4083−4095.
(39) Isborn, C. M.; Leclerq, A.; Vila, F. D.; Dalton, L. R.; Bredas, J. L.; Eichinger, B. E.; Robinson, B. H. *J. Phys. Chem. A* **2007**, *111*, 1319−1327.

The dendritic chromophores, relative to undressed chromophores dispersed in polymer, have a larger r_{33} coefficient because of the stability of the material under poling. The design paradigm of chromophores covalently attached in a local network appears to overcome the frustration commonly observed in dipolar glasses that has previously limited the maximum achievable chromophore density and resultant electro-optic activity. However the degree of order observed in these systems is still well below that of the theoretical maximum predicted by analytic theory. Subtle changes in molecular architecture may be able to minimize the inter- and intramolecular electrostatic interactions that attenuate order, leading to materials with previously unrealized electro-optic activity. The framework of the MC calculations presented herein provide a tool for quickly assessing the influence of changes in molecular architecture on the overall structure of bulk ONLO materials. It is our hope that the work presented will accelerate the development of new optical materials and devices through the careful integration of theory, experiment, and rational design.

Experimental Section

General Synthesis. All solvents were purified by distillation prior to use unless otherwise stated. Commercially available chemicals were used as received unless otherwise stated. All alkylithium reagents were titrated prior to use. Glassware was base treated and oven or flame dried. All reactions were performed under inert atmosphere. Amorphous polycarbonate, APC (poly[bisphenol A carbonate-co-4,4′-(3,3,5-trimethylcyclohexyl-idene)diphenol carbonate]), was purchased from Sigma Aldrich and purified by repeated precipitaion from a THF solution into methanol followed by filtration and vacuum drying before use.

2-[4-(2-{5-[2-(4-{[2-(*tert*-Butyl-dimethyl-silanyloxy)-ethyl]-methyl-amino}-phenyl)-vinyl]-3-hydroxymethyl-thiophen-2-yl}-vinyl)-3-cyano-5-phenyl-5-trifluoromethyl-5*H*-furan-2-ylidene]-malononitrile (Chromophore 1). This compound was prepared following literature procedures that were slightly modified to include a single hydroxy−ethyl donor functionality for attachment of the outer dendron in PSLD_41. Complete synthetic details are available online in the Supporting Information.[19,20]

1,1,1-Tris-(6-hexanoic acid-4-phenyl) Ethane (2). The triacid dendrimer core was synthesized according to literature procedure.[19]

Dendrimer PSLD_33. An oven dried, magnetically stirred, 100 mL two-neck round-bottomed flask was charged with 1,1,1-Tris-(6-hexanoic acid-4-phenyl) ethane (**2**) (0.221 g, 0.341 mmol), chromophore (**1**) (0.820 g, 1.13 mmol), 1,3-dicyclohexylcarbodiimide (0.260 g, 1.26 mmol), and DPTS (0.10 g, 0.341mmol). After 1 h of drying under a high vacuum, the mixture was dissolved in freshly distilled THF (10 mL) and DCM (15 mL). The reaction was stirred for 48 h and washed with NaCl (saturated), and the organic layer was collected. The aqueous layer was extracted with DCM, and the combined organics were washed with water, dried over $MgSO_4$, and condensed in vacuo. The dark-blue crude solid was purified by silica gel column chromatography (5% THF/ DCM) to yield 0.477 g (50%) of a deep blue solid. ^{1}H NMR (300 MHz, $CDCl_3$): δ 7.89 (J = 15.3 Hz), 7.58-7.54 (m, 15H), 7.39 (d, J = 9 Hz, 6H), 7.13 (d, J = 15.9 Hz, 3H), 7.03 (s, 3H), 6.98, (d, J = 8.7 Hz, 6H), 6.96 (d, J = 15.9 Hz, 3H), 6.77 (d, J = 8.7 Hz, 6H), 6.68 (d, J = 8.7 Hz, 6H), 6.64 (d, J = 15.3 Hz, 3H), 4.92 (d, J = 3 Hz, 6H), 3.94 (t, J = 6.3 Hz, 6H), 3.81 (t, J = 6 Hz, 6H), 3.56 (t, J = 6 Hz, 6H), 3.10 (s, 9H), 2.35 (t, J = 7.2 Hz, 6H), 2.09 (br-s, 3H), 1.87-1.79 (m, 6H), 1.72-1.67(m, 6H), 1.55-1.49 (m, 6H), 0.89 (s, 27H), 0.03 (s, 18H), ppm. MALDI-TOF: m/z calcd 2780.04; found, [M + Na], 2804.476 (m/z). Anal. Calcd for $C_{155}H_{159}F_9N_{12}O_{15}S_3Si_3$: C, 66.93; H, 5.76; N, 6.04%. Found: C, 67.92; H, 5.96; N, 5.89%. UV−vis: λ_{max} ($CHCl_3$) = 759 nm; λ_{max} (film) = 734 nm. DSC: T_g = 96 °C

Deprotection of PSLD_33 (3). A 50 mL round-bottomed flask is charged with PSLD_33 (0.19 g) and acetone was added to dissolve (4 mL). HCl (1 N, 0.5 mL) was then added. The reaction was allowed to proceed for 2.5 h. The mixture was then neutralized with $NaHCO_3$, and the product was collected by filtration. The blue solid was obtained in quantitative yield and used without further purification. ^{1}H NMR (300 MHz, $CDCl_3$): δ 7.91 (d, J = 15 Hz, 3H), 7.58-7.52 (m, 15H), 7.37 (d, J = 8.7 Hz, 6H), 7.08 (d, J = 15.6 Hz, 3H), 7.01 (s, 3H), 6.96 (d, J = 8.7 Hz, 6H) 6.93 (d, J = 15.3 Hz, 3H), 6.77-6.74 (m, 12H), 6.60 (d, J = 15.3 Hz, 3H), 4.91 (s, 6H), 3.95 (t, J = 6.3 Hz, 6H), 3.86 (t, J = 5.4 Hz, 6H), 3.6 (t, J = 5.4 Hz, 6H), 3.09 (s, 9H), 2.35 (t, J = 7.5 Hz, 6H), 2.08 (s, 3H), 1.83-1.74 (m, 6H), 1.72-1.64 (m, 6H), 1.54-1.45 (m, 6H) ppm. MALDI-TOF: m/z calcd 2437.78; found, [M + H], 2438.1, [M+Na], 2461.040 (m/z).

Dendrimer PSLD_41. An oven dried, magnetically stirred, 100 mL two-neck round-bottomed flask was charged with **3** (0.10 g, 0.041 mmol), dendron 1 (**FD**) (0.084 g, 0.164 mmol), 1,3-dicyclohexylcarbodiimide (0.038 g, 0.184 mmol), and DPTS (0.030 g, 0.20 mmol). After 1 h of drying under a high vacuum, the mixture was dissolved in freshly distilled THF (10 mL) and DCM (15 mL). The reaction was stirred for 48 h and washed with NaCl (saturated), and the organic layer was collected. The aqueous layer was extracted with DCM, and the combined organics were washed with water, dried over $MgSO_4$, and condensed in vacuo. The dark-blue crude solid was purified by silica gel column chromatography (2.5% THF/DCM) to yield 0.1 g (0.025 mmol, 62%), of a deep-blue solid. ^{1}H NMR (500 MHz, $CDCl_3$): δ 7.93, (d, J = 15.5, 3H), 7.58-7.54 (m, 15H), 7.39 (d, J = 9 Hz, 6H), 7.21 (d, J = 2.5 Hz, 6H), 6.99 (s, 3H), 6.98 (d, J = 7 Hz, 6H), 6.96 (d, J = 15.5 Hz, 3H), 6.87 (d, J = 15.5 Hz, 3H), 6.83 (d, J = 9 Hz, 6H), 6.77 (d, J = 9 Hz, 6H), 6.71 (t, J = 2.5 Hz, 3H), 6.66 (d, J = 15.5 Hz, 3H), 4.99 (s, 12H), 9.86 (dd, J_1 = 13 Hz, J_2 = 6.5 Hz, 6H), 4.54 (t, J = 5.5 Hz, 6H), 3.93 (t, J = 6.5 Hz, 6H), 3.86 (t, J = 5.5 Hz, 6H), 3.13 (s, 9H), 2.36 (t, J = 7.5 Hz, 6H), 2.09 (br-s, 3H), 1.82-1.76 (m, 6H), 1.73-1.67 (m, 6H), 1.53-1.47 (m, 6H), ppm. MALDI-TOF: m/z calcd 3926.83; found, [M + H], 3927.26, [M + Na], 3950.25 (m/z). Anal. Calcd for $C_{200}H_{135}F_{39}N_{12}O_{24}S_3$: C, 61.16; H, 3.46; N, 4.28%. Found: C, 60.86; H, 3.25; N, 4.46%. UV−vis: λ_{max} ($CHCl_3$) = 726 nm; λ_{max} (film) = 720 nm. DSC: T_g= 103 °C

Thin Film Fabrication Techniques and EO Measurements. Real time pole and probe r_{33} measurement details have been reported previously.[19] Samples of each material were prepared by solution spin-casting onto ITO-coated glass slides gold electrodes ($d \approx 200$ nm) were then deposited atop the films. EO measurements were performed at λ = 1300 nm, and r_{33} measurements were recorded after cooling and removal of the poling field. Values were calculated by sine-wave fitting of lock-in-amplifier and direct current detector response curves as a function of the relative phase angle (Ψ_{sp}) between T_E and T_M. Values for r_{33} were then calculated from I_c and I_m values using

$$r_{33} = \frac{3\lambda I_m}{4\pi V_m I_c n^2} \frac{(n^2 - \sin^2\theta)^{1/2}}{\sin^2\theta} \propto I_m/I_c$$

where V_m is measured directly at the sample electrodes during poling.[20]

Acknowledgment. The authors acknowledge the support of the STC-MDITR Program of the National Science Foundation (Grant DMR0120967) and NSF (Grant DMR-0092380). Support from the Air Force Office of Scientific Research under AFOSR-(F49620-03-1-0110-P000), as well as from the DARPA MORPH program Phase I ((N) 14-04-10094), is also gratefully acknowledged.

Supporting Information Available: Complete synthetic and characterization details for chromophore 1 as well as representative thermal and refractive index analyses. This material is available free of charge via the Internet at http://pubs.acs.org.

JA068322B